



Quantifying farmed kelp atmospheric CO₂ uptake through localized air-sea flux in the Northern Gulf of Alaska

Josianne Haag¹, Cale A. Miller², Jonah Jossart¹, Amanda L. Kelley¹

¹College of Fisheries and Ocean Sciences, University of Alaska Fairbanks, Fairbanks, AK, 99775, USA

5 ² Department of Earth Sciences, Geosciences, Utrecht University, 3508 TC, The Netherlands

Correspondence to: Josianne Haag (jhaag6@alaska.edu)

Abstract. The rapid growth of mariculture in the United States, particularly in Alaska, has ignited interest in the co-benefit of using farmed kelp as a mitigation strategy against anthropogenic carbon dioxide (CO₂) released to the atmosphere. Here, we quantified the air-sea CO₂ flux in three kelp farms across the Northern Gulf of Alaska with differing oceanographic conditions and farming practices to determine the carbon sequestration potential over the growing season. Sensors were deployed on two subsurface moorings placed in proximity of one another at each farm site: one “inside” and one “outside” as a control upstream of the farm. Both sensor arrays conducted hourly measurements of pH or CO₂, temperature, salinity, and oxygen during the time from seed line outplanting in winter (November to January) to spring harvest (April or May) in 2024. Nominal differences in carbonate chemistry parameters were detected between the inside and outside moorings until March, when the frequency of variability remained consistent between moorings but their respective magnitude diverged. Notably, apparent oxygen production, seawater CO₂ concentration, air-sea CO₂ flux, and strength of periodic signals varied by farm site. Integrated over the entire deployment, two farms demonstrated net negative air-sea CO₂ fluxes while one served as a net source of carbon: $-84,397 \pm 41,374$ mol m² in Jakolof Bay, $-11,115 \pm 1,331$ mol m² in Kalsin Bay, and 543 ± 21 mol m² in Windy Bay. This study highlights the nuance of farmed kelp carbon capture by demonstrating that farm site can influence overall air-sea CO₂ flux and that kelp farms are not always a net sink for atmospheric carbon.

1 Introduction

Since the Industrial Revolution, the global ocean has absorbed almost one-third of anthropogenically produced CO₂ (Feely et al. 2004; Quéré et al. 2018), driving a process termed ocean acidification. OA has direct and indirect deleterious effects on marine organisms such as shell dissolution in crustaceans and mollusks (Ries et al. 2016), malfunctioning olfactory responses in salmon (Williams et al. 2019), and stunted growth and development across trophic levels (Kurihara et al. 2013; Bignami et al. 2013; Long et al. 2013; Alcantar et al. 2024). If elevated CO₂ emissions to the atmosphere are not reduced, the poorest and most vulnerable human populations are most likely to suffer losses and damages as a result (IPCC 2022). To help curtail the impacts of these climactic changes, efforts to sequester carbon in ocean environments have been proposed and referred to as marine carbon dioxide removal (mCDR). mCDR methods aim to enhance the flux of CO₂ into the ocean



through techniques such as ocean fertilization, ocean alkalization enhancement, artificial upwelling, and kelp carbon sequestration (DeAngelo et al. 2023; Oeschlies et al. 2025).

The burial of biomass from highly productive organisms, such as seaweed, has shown promise as a sustainable option for capturing carbon through enhanced photosynthesis (Jiang et al. 2013; Ikawa and Oechel 2015). A recent study characterized the average rate of organic carbon burial in sediments at 20 seaweed farms at $2.41 \pm 1.68 \text{ mmol C m}^{-2} \text{ yr}^{-1}$, placing seaweed farms on the low end of burial rates in natural marine carbon sinks (Duarte et al. 2025). While the nearshore environment generally acts as a source of CO_2 to the atmosphere due to net heterotrophy (Chen and Borges 2009; Cai 2011), many kelp farms around the world have demonstrated that atmospheric CO_2 can be taken up by kelp and converted into seaweed biomass (Ikawa and Oechel 2015; Jiang et al. 2015; Mongin et al. 2016). For the ocean to effectively absorb atmospheric CO_2 , atmospheric CO_2 levels must be in disequilibrium with the ocean, which is dependent on factors such as wind and temperature (Wanninkhof 2014). In Lido town, China, a kelp farm exhibited variation in net autotrophic activity throughout the year with the greatest drawdown of atmospheric CO_2 in spring and the least amount in summer (Jiang et al. 2013). However, to achieve climate benefits, kelp farming would need to expand significantly, covering over 90,000 km^2 (Coleman et al. 2022; DeAngelo et al. 2023). Furthermore, seaweed would need to absorb an estimated 4 Gt $\text{CO}_2 \text{ yr}^{-1}$ to achieve net zero emissions by 2050, though considerable uncertainty remains around these estimations (Arzeno-Soltero et al. 2023). Given the scale of such efforts, other, more logistically feasible approaches have been proposed, such as implementing the use of kelp farms to locally reduce atmospheric CO_2 concentrations by shifting the magnitude and timing of carbon cycling.

The Northern Gulf of Alaska (NGA) has been identified as a potential site for scaling up kelp farming due to its vast coastline, highly productive waters, and the need to help transition the state economy away from heavy reliance on fossil fuel extraction and unpredictable wild fish stocks (Miller 2021; Bullen et al. 2024; Edgar et al. 2024). As a result, the NGA kelp farming industry expects to expand dramatically in the next two decades, increasing sustainable economic practices in the state with the added benefit of enabling the coastal system to potentially take up excess atmospheric CO_2 . Empirical rate estimates of CO_2 drawdown by kelp from other regions are not universally applicable, due to the site-specific interaction of many physical and biological factors that affect kelp-related CO_2 flux rates (Ikawa and Oechel 2015; Jiang et al. 2015; Mongin et al. 2016). Accordingly, Alaska-specific values are needed, so that we may better assess the climate benefits of kelp farming in the NGA.

In the NGA, seeded lines are deployed between October and January, and harvested in late spring before biofouling by epiphytic organisms (Stekoll et al. 2021). Coastal marine ecosystems in the NGA are generally net heterotrophic, aside from approximately sixty days of net autotrophy in summer and early fall (Miller and Kelley 2021); however, on the continental shelf, the ocean acts primarily as a carbon sink (Evans and Mathis 2013). Currently, there are no estimates of kelp farm air-sea CO_2 fluxes in the NGA, although nearshore macroalgal-dominated habitats can alter carbonate chemistry and create seasonal, localized carbon sinks, signaling the potential to utilize farmed seaweed as one mechanism to reduce



atmospheric CO₂ concentrations (Miller and Kelley 2021). This study quantified the air-sea CO₂ flux in three kelp farms across the NGA to determine the capacity of farmed kelp to take-up CO₂ relative to adjacent waters. This study provides empirical estimates of kelp farm-related CO₂ flux, thus identifying the role that Alaska's kelp farming industry can play in reducing atmospheric CO₂ and highlighting the capacity of farms to offset anthropogenic CO₂ emissions.

2 Materials and methods

2.1 Site descriptions

Three nearshore kelp farms were selected across the Northern Gulf of Alaska (NGA) spanning a distance of over 400 km: Spinnaker Sea Farms in Jakolof Bay (59.4604 °N, 151.5193 °W), Royal Ocean Kelp Co in Windy Bay (60.5628 °N, 145.9569 °W), and Alaska Ocean Farms in Kalsin Bay (57.6581 °N, 152.4201 °W) (Fig. 1). The three farm sites varied in size, harvest period, and species grown. Spinnaker Sea Farms in Jakolof Bay covered 7,500 m² and grew *Saccharina latissima* and *Alaria marginata*. The farm also cultivated Pacific oysters (*Crassostrea gigas*) in lantern nets and metal cages on a longline on the inner side of the farm. Seed lines (i.e., lines populated with young sporophytes) were outplanted in December and harvested in late April. The average water column depth at the farm shifted from 5.5 m to 10 m depending on the tide. Due to elevated light availability associated with the shallow water column across the entirety of Jakolof Bay, the muddy to rocky benthos is covered with wild *S. latissima*. Alaska Ocean Farms in Kalsin Bay, in operation for three years, covered 3,200 m² and grew only *A. marginata*. Seed lines were outplanted in January and harvested in late May. The depth of the site varied from 9 to 18 m with a tidal range of up to 3 m. The substrate was largely composed of sand. Royal Ocean Kelp Co in Windy Bay covered 12,000 m² and contained two catenary arrays: one of *S. latissima* and one of *A. marginata* suspended at approximately 2.2 m and 1.2 m depth, respectively. The eight lines making up each array were spaced 3 m apart. Seed lines were outplanted in October and harvested in early May. The water column depth at the farm varied from 12 m to 22 m with a tidal range of 5.5 m. The substrate was largely made up of mud. None of these sites are glacier-influenced.

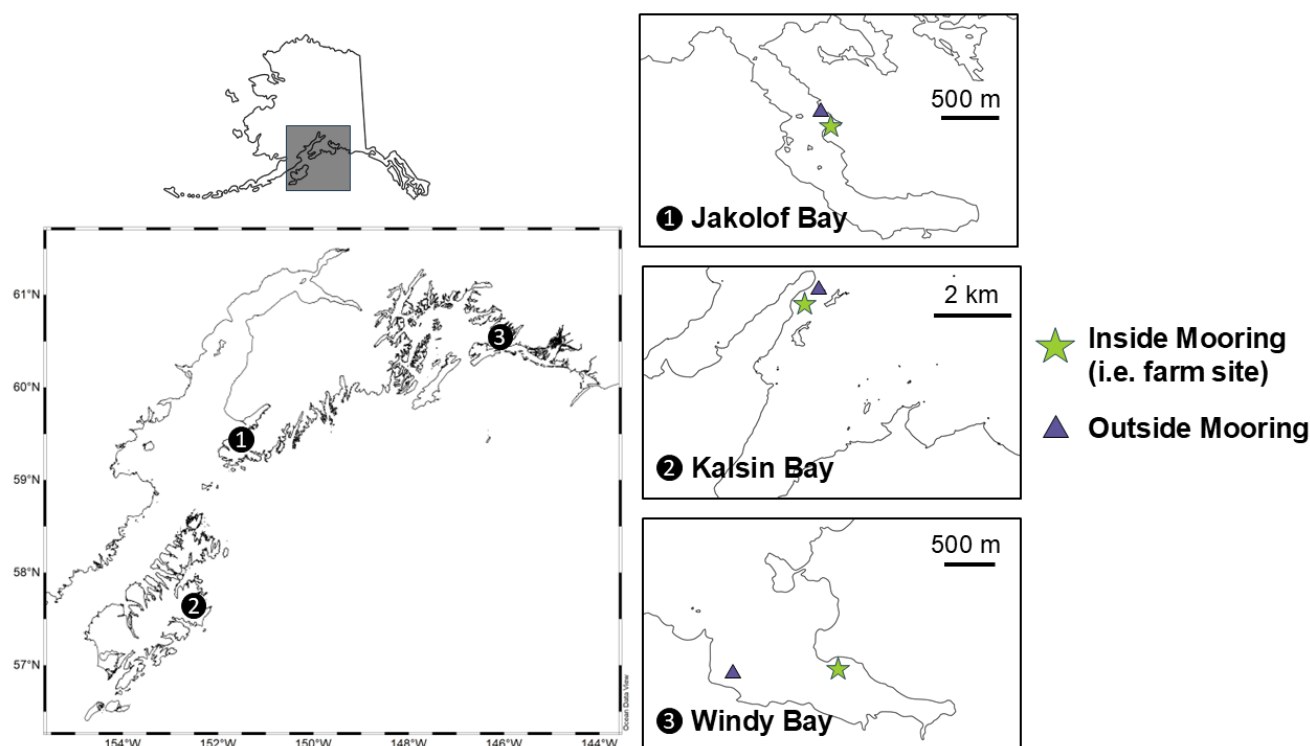


Figure 1: Map of the kelp farm study sites: Spinnaker Sea Farms in Jakolof Bay, Alaska Ocean Farms in Kalsin Bay, and Royal Ocean Kelp Co. in Windy Bay. An “inside mooring” was deployed within the farm and an “outside mooring” was deployed upstream of the farm to act as a control for background respiration and photosynthesis. The distance between these moorings was 50 m in Jakolof Bay, 100 m in Kalsin Bay, and 600 m in Windy Bay. All arrays suspended 3 m below the surface, roughly the depth of the growing kelp.

2.2 Sensor deployments, calibrations, and carbonate system calculations

A sensor array was deployed inside and outside of each farm (Fig. 1). To accurately estimate net air-sea CO_2 flux of kelp farms through time, the outside mooring must be influenced by the same water mass as the farm to capture background photosynthesis and respiration. In general, the “inside” sensor array was positioned as close to the center of the farm as possible and supported by a buoy. The “outside” sensor array was placed on a mooring a distance from the farm to ensure that it was not influenced by the biological activity of the farm while still experiencing the same water masses (Fig. 1). Given the different bathymetric and hydrologic features at each farm site, placement distance between the arrays varied; however, the depth of both the inside and outside mooring within the water column were similar across sites. Each sensor array was outfitted with a minimum of a Sea-Bird SeapHOxTM (combination of the SeaFETTM pH sensor and the SBE 37-SMP-ODO MicroCAT CTD+DO sensor) or a Sunburst SAMI-CO₂TM, a PME miniDOT optical oxygen logger, and an Onset HOBO conductivity logger. The sensor arrays were suspended roughly 3 m from the surface, which is the same depth as the growing kelp. All parameters were measured on a frequency of one hour.



Calibration and reference seawater bottle samples were collected by farmers when they visited their farms by lowering a Science First™ 1.5L Water Sampler to the depth of the sensor array and filling 250 mL borosilicate bottles pre-spiked with 200 µL saturated mercuric chloride. During the retrieval of the sensors at each site in spring/summer, a survey was conducted to capture within-farm spatial variability in carbonate chemistry by collecting water samples in a grid formation at the depth of the kelp using the same methods as above. The discrete bottle samples were analyzed for pH_T (total scale) if complementing the pH sensors or dissolved inorganic carbon (DIC) if complementing the CO_2 sensors, and all samples were analyzed for total alkalinity (TA) and salinity. A Shimadzu 1800 spectrophotometer was used to measure seawater pH_T using meta-cresol purple as an indicator dye (Acros, batch #30AXM-QN), and applying a dye impurity correction factor (Douglas and Byrne 2017). A DIC Analyzer (Model AS-C6L) coupled to a LI-7815 $\text{CO}_2/\text{H}_2\text{O}$ Analyzer measured DIC using a three-point calibration of Certified Reference Material (CRM: Batch 172, A.G. Dickson, Scripps Institute of Oceanography). A Metrohm 848 Titrino plus measured TA via an open-cell titration and a YSI 3100 Conductivity instrument measured salinity.

The SeaFETs were calibrated using the pH_T measured from the discrete seawater samples by calculating electrode specific single-point calibration coefficients, which were then used to derive the entire pH dataset (Bresnahan et al. 2014; Miller et al. 2018). The HOBO loggers were calibrated with the HOBOWare® Pro software using the salinity and temperature measured by either the CTD within the SeapHOx or with the discrete bottle samples. The SAMI- CO_2 timeseries was translated up or down relative to the discrete water samples. The miniDOTs were calibrated using the mean atmospheric pressure and salinity over the deployment. Data can be accessed from the DataONE repository (<https://doi.org/10.24431/rw1k9hb>).

Calculations were conducted in R (version 4.4.1) and MATLAB (version R2024b). The uncertainty associated with the pH_T timeseries was calculated following Bresnahan et al. (2024) and Miller and Kelley (2021). In short, the propagated uncertainty incorporated all sources of possible error in the sample analysis procedure: the difference in the lab measurement of pH_T and TA on a known CRM bottle versus the expected values, the standard deviation of the duplicate calibration bottle measurements, and the constants error for the CO_2Sys conversions (version 2.3; Lewis and Wallace 1998). Total uncertainty was calculated by adding the propagated uncertainty to the difference between a reference bottle and the calibrated pH timeseries (following Miller and Kelley 2021). The pH uncertainty was then converted to an in situ partial pressure of CO_2 ($p\text{CO}_2$) uncertainty using a Monte Carlo simulation whereby the pH uncertainty was used to create a series of perturbed pH values for each timepoint ($n = 10,000$) that were then converted to $p\text{CO}_2$ using the ‘seacarb’ package in R (version 3.3.3; Gattuso et al. 2015). When summarizing the timeseries data and spatial survey to single means, the standard deviation was reported to capture the natural variability of the value and not the total uncertainty.

The ‘seacarb’ package can estimate any carbonate system parameters using two known values. The calibrated pH timeseries was used in Jakolof Bay and Windy Bay as the first variable, while $p\text{CO}_2$ was used in Kalsin Bay. The second variable across all sites was TA calculated from salinity using a known salinity-TA relationship for the nearshore of the NGA (Evans et al. 2015; see Fig. A1). The $p\text{CO}_2$ timeseries was subsequently used to calculate air-sea CO_2 fluxes (FCO_2) following Eq. 1 by Wanninkhof (2014):



$$FCO_2 = 0.251U^2(Sc/660)^{-0.5}K_0(pCO_{2w} - pCO_{2a}) , \quad (1)$$

where U is the wind speed in $m\ s^{-1}$, $Sc/660$ is the dimensionless Schmidt number, K_0 is the Bunsen solubility coefficient with units of $mol\ L^{-1}\ atm^{-1}$, and pCO_{2w} and pCO_{2a} are the pCO_2 in water and air, respectively. Site-specific wind data was obtained from the NOAA Buoy Data Center (2024) and pCO_{2a} was assumed to be ~ 421.2 ppm at all sites (McKain et al. 2024). $Sc/600$ and K_0 were calculated using the polynomial equations in Wanninkhof (2014). In the absence of wind, the above equation becomes simplified as per MacIntyre (1995) to:

$$FCO_2 = 0.8K_0(pCO_{2w} - pCO_{2a}), \quad (2)$$

since atmospheric exchange continues even when turbulent mixing at the water surface does not occur. The net FCO_2 was calculated by subtracting the FCO_2 estimated for the inside mooring from the outside mooring for each farm site location and integrating over the entire timeseries. An uncertainty for total net integrated FCO_2 was calculated by propagating the errors associated with each of the sensors and the data pulled from online resources through the air-sea flux calculation and integration.

2.2 Ancillary data analysis

Temperature-salinity (T-S) diagrams were used to determine if the inside and outside moorings experienced the same water mass, since a water mass can be defined by their salinity and potential temperature as those variables remain conserved unless experiencing mixing conditions. T-S diagrams were created by modifying the ‘ggTS’ function (Kaiser 2020), which utilized the ‘gsw’ package to calculate the potential density and plot isopycnals (version 1.2-0; Kelley et al. 2024). Similarities between the T-S diagrams for both moorings would indicate that the outside mooring can act as a control for the inside mooring. The lag time between the outside and inside moorings were characterized by detrending the data and applying a cross-correlation using the ‘tseries’ package (version 0.10-58; Trapletti et al. 2015).

The timeseries at each site was divided into three phases in order to compare carbonate chemistry shifts throughout the kelp growing season: heterotrophy, transitional, and autotrophy. Net heterotrophy or autotrophy of seawater was determined by calculating the apparent oxygen production (AOP) across the timeseries, which is the difference between the measured *in-situ* oxygen versus the estimated oxygen saturation as a function of temperature and salinity (Garcia and Gordon 1992: equations corrected from Casamitjana and Roget 1993). The shift from heterotrophy or autotrophy to the transitional phase was characterized as the first twenty-four-hour period in which average daily AOP shifted from positive to negative or vice versa, and the shift from the transitional phase back to either heterotrophy or autotrophy was characterized as a period of time when daily averaged AOP remained either positive or negative for over one week.

The drivers of seawater pCO_2 were assessed by doing a decomposition of monthly averages of pCO_2 based on the effects of temperature (T), salinity (S), total alkalinity (TA), air-sea CO_2 flux (FCO_2), and dissolved inorganic carbon (DIC). The



following equations were modified from Garcia-Troche et al. (2021), originally based on pH, to describe observed monthly changes between two consecutive months (t_1 and t_2):

$$\Delta pCO_2 = \Delta pCO_2(T) + \Delta pCO_2(S) + \Delta pCO_2(TA) + \Delta pCO_2(FCO_2) + \Delta pCO_2(DIC) + R, \quad (3)$$

170 where a change in seawater pCO_2 from one month to another (ΔpCO_2) can be described as the changes to the five variables plus a residual (R), which represents any remaining ΔpCO_2 not explained by T, S, TA, FCO_2 , or DIC. Using the ‘seacarb’ package in R, the stepwise calculated change in pCO_2 between t_1 and t_2 was derived by a single variable at a time to calculate the monthly $\Delta pCO_2(T)$, $\Delta pCO_2(S)$, and $\Delta pCO_2(TA)$:

$$\Delta pCO_2(T) = \Delta pCO_{2,2}(T_2, S_1, TA_1, DIC_1) - \Delta pCO_{2,1}, \quad (4)$$

$$\Delta pCO_2(S) = \Delta pCO_{2,2}(T_1, S_2, TA_1, DIC_1) - \Delta pCO_{2,1}, \quad (5)$$

175 $\Delta pCO_2(TA) = \Delta pCO_{2,2}(T_1, S_1, TA_3, DIC_1) - \Delta pCO_{2,1}, \quad (6)$

Due to DIC exerting an effect on both $\Delta pCO_2(FCO_2)$ and $\Delta pCO_2(DIC)$, as a result of air-sea CO_2 exchange and water column/benthic processes, respectively, $\Delta pCO_2(FCO_2)$ was calculated first and subsequently used to separate its signal from $\Delta pCO_2(DIC)$. $\Delta pCO_2(FCO_2)$ required an estimate of monthly CO_2 air-sea exchange calculated using Eq. 1 and 2 (i.e., FCO_2), the change in time ($t_2 - t_1$, days), seawater density (d , $kg\ m^{-3}$), and sampled depth (H , m) from Garcia-Troche et al. (2021):

180 $\Delta DIC_{air-sea} = \frac{-FCO_2 \times (t_1 - t_2)}{d \times H}, \quad (7)$

$$\Delta pCO_2(FCO_2) = \Delta pCO_{2,2}(T_1, S_1, TA_1, DIC_1 + \Delta DIC_{air-sea,2}) - \Delta pCO_{2,1}, \quad (8)$$

$$\Delta pCO_2(DIC) = \Delta pCO_{2,2}(T_1, S_1, TA_1, DIC_2) - \Delta pCO_2(FCO_2) - \Delta pCO_{2,1}, \quad (9)$$

The monthly periodicity of pCO_2 was estimated with a power spectral analysis using R package ‘spectrum’ (version 1.1; John and Watson 2020). The span was set to 20 days. A high-pass Butterworth filter (package ‘signal’; version 1.8-1; Ligges et al. 2015) was first applied to remove low-frequency components that can dominate the spectrum. The cutoff was set to 0.01 cycles per hour. The underlying periodicities were plotted to visually determine the dominant drivers of pH_T frequency.

185

3 Results

3.1 Comparison of inside and outside moorings

Comparison of water mass movement at the inside and outside moorings confirmed that both sensor arrays detected similar water masses, allowing for a calculation of net air-sea CO_2 flux when paired with the inside sensor array. T-S diagrams were remarkably similar between inside and outside moorings across all sites, with distinct shifts through time driven by temperature, denoted in the color overlay (Fig. 2). Salinity remained relatively consistent through the deployment period (30.9 ± 0.4 in Jakolof Bay, 30.0 ± 0.6 in Kalsin Bay, and 31.1 ± 0.4 in Windy Bay) while temperature at all three sites

190



decreased from winter to early spring before warming once again (Fig. 2). The inflection of temperature warming occurred at different times depending on the site: early March in Jakolof Bay, mid-March in Kalsin Bay, and mid-April in Windy Bay. The cross-correlations measured between salinity and temperature at the paired moorings indicate a lag time of 0 hours in Jakolof Bay, 1 hour according to salinity and 0 hours according to temperature in Kalsin Bay, and 1 hour in Windy Bay for both variables, demonstrating strong similarities at the inside and outside moorings.

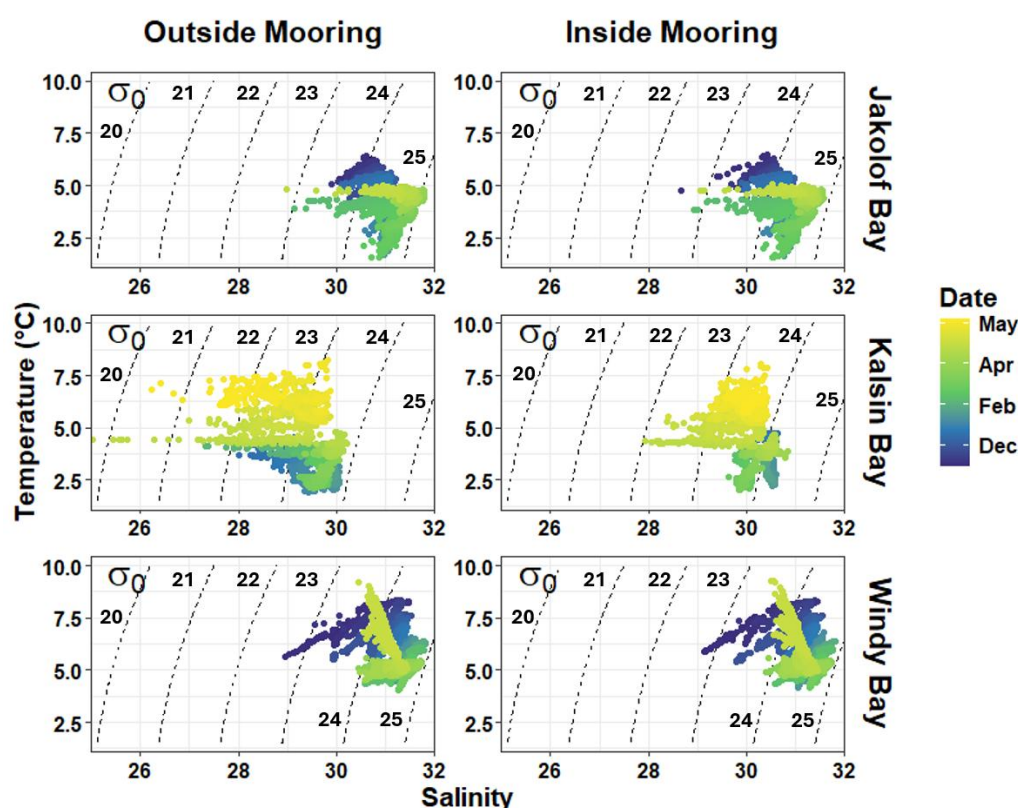
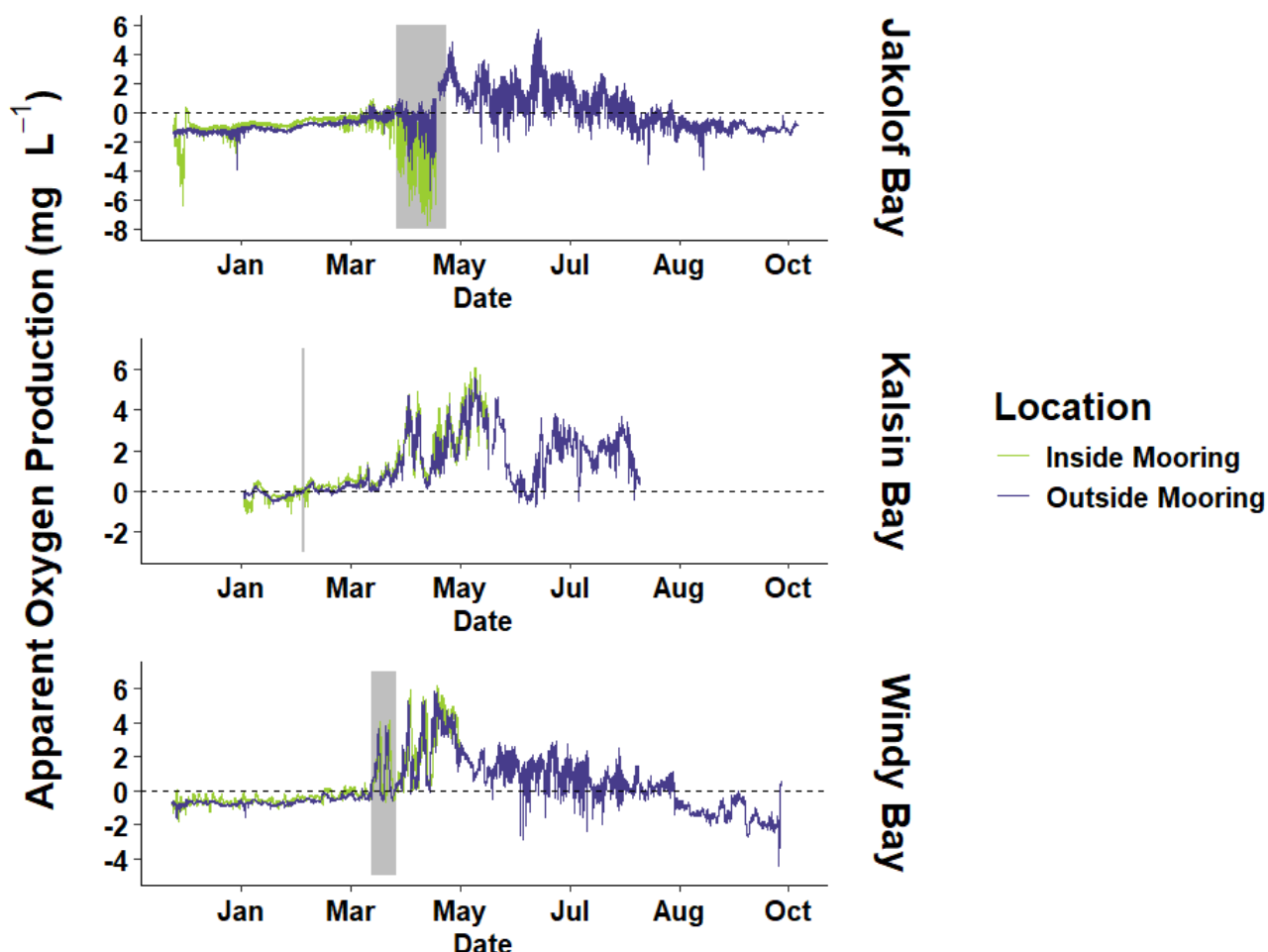


Figure 2: Temperature-salinity diagrams from three locations in the Northern Gulf of Alaska at moorings within kelp farms (inside moorings) and control moorings upstream of the farm sites (outside moorings). Sensor arrays collected hourly data from 3 m depth. Labelled dashed lines denote isolines of potential density (σ_0 ; -1000 kg m^{-3}).

Apparent oxygen production (AOP), the difference between *in situ* O_2 and O_2 saturation estimated as a function of temperature and salinity, demonstrated that the nearshore systems at each site experienced a distinct shift from net heterotrophy to net autotrophy throughout the growing season (Fig. 3). All sites began with net heterotrophy in winter and, as spring progressed, neared the solubility compensation point ($\text{AOP} = 0$) where the system shifted to a transitional phase (on April 2 in Jakolof Bay, February 13 in Kalsin Bay, and March 20 in Windy Bay). The length of this transitional phase varied depending on location: 23 days in Jakolof Bay, 0 days in Kalsin Bay, and 13 days in Windy Bay. Kalsin Bay and Windy Bay



210 became net autotrophic during the kelp growing season on February 13 and April 2, respectively, while Jakolof Bay remained near the solubility compensation point until after kelp harvest (Fig. 3). The inside mooring demonstrated greater net heterotrophy than the outside mooring in Jakolof Bay starting in late March. In Windy Bay and Kalsin Bay, the inside mooring was characterized by higher net autotrophy than the outside mooring as time neared harvest (Fig. 3).



215 **Figure 3: Apparent oxygen production (i.e. measured O_2 minus saturated O_2) across the farmed kelp growing season and the following summer in Jakolof Bay, Kalsin Bay, and Windy Bay both inside the farm (inside mooring) and at the control site outside of the farm (outside mooring). The dashed line indicates when measured O_2 is equal saturated O_2 and thus denotes the solubility compensation point. The grey boxes indicate the transitional period from net heterotrophy to net autotrophy in spring.**

During the net heterotrophic wintertime phase described by AOP, all three timeseries displayed ambient seawater (i.e. the
220 outside mooring) pCO_2 values greater than atmospheric CO_2 (i.e. $421.2 \mu atm$; McKain et al. 2024; Fig. 4). In Windy Bay, the inside and outside moorings had associated total uncertainties of $69.46 \mu atm$ and $73.73 \mu atm$, respectively, and in Jakolof Bay, the inside and outside moorings had associated total uncertainties of $93.45 \mu atm$ and $91.06 \mu atm$, respectively. The



average $p\text{CO}_2$ at the outside mooring during this net heterotrophic period was $448.2 \pm 21.9 \mu\text{atm}$ for Jakolof Bay ($n = 2812$), and $482.2 \pm 22.4 \mu\text{atm}$ for Windy Bay ($n = 2854$). Note that the $p\text{CO}_2$ data in Kalsin Bay began during the autotrophic period (Fig. 4). From the beginning of the transitional period to kelp harvest, seawater $p\text{CO}_2$ decreased below atmospheric CO_2 at two of the three sites, Kalsin Bay and Windy Bay, with a concurrent increase in $p\text{CO}_2$ variability (Fig. 4). The total average $p\text{CO}_2$ at the outside mooring during this time was $317.5 \pm 91.3 \mu\text{atm}$ for Kalsin Bay ($n = 2133$) and $306.1 \pm 99.3 \mu\text{atm}$ for Windy Bay ($n = 1145$). In contrast, in Jakolof Bay the total average $p\text{CO}_2$ at the outside mooring was $604.2 \pm 370.1 \mu\text{atm}$ ($n = 522$) with a maximum of $2958.4 \mu\text{atm}$ in late April. It must be noted that the moorings in Jakolof Bay were heavily colonized by wild kelp, whereas biofouling at the other two sites was minimal (see Fig. A2).

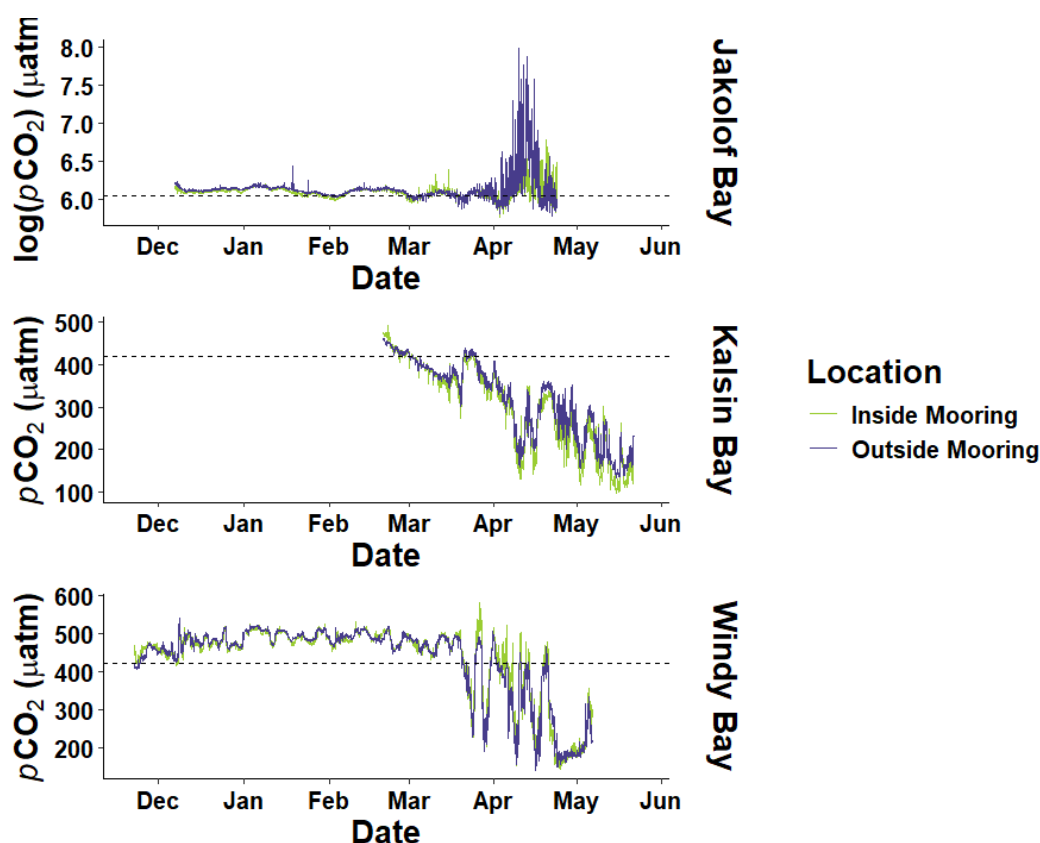


Figure 4: The partial pressure of carbon dioxide ($p\text{CO}_2$) in seawater inside and outside of kelp farms across the kelp growing season in Jakolof Bay (note the log axis), Kalsin Bay, and Windy Bay. The dashed line indicates the atmospheric CO_2 value which has been estimated to be $\sim 421.2 \text{ ppm}$ at all sites (McKain et al. 2024).

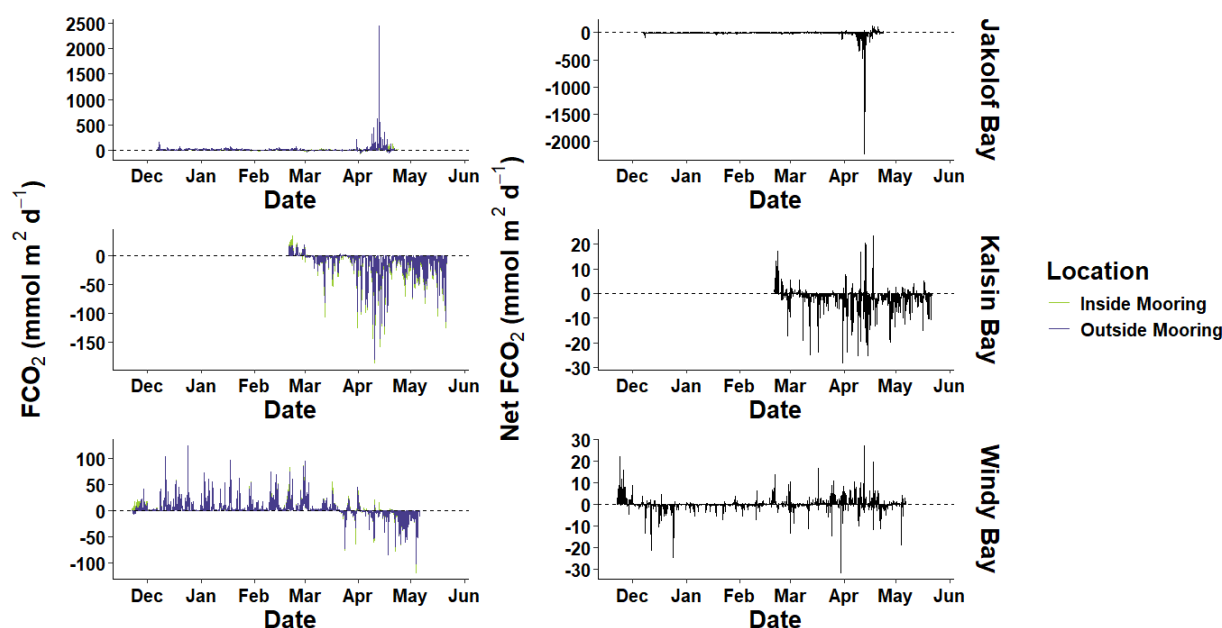
The variability in $p\text{CO}_2$ was consistent between the inside and outside moorings throughout the entire deployment period, although after shifting from heterotrophy to autotrophy, the magnitude of variability increased at the inside mooring, clearly indicating the influence of kelp (Fig. 4). During the wintertime net heterotrophic phase, the absolute difference in $p\text{CO}_2$ at the inside versus outside moorings differed an average of $10.1 \pm 10.0 \mu\text{atm}$ in Jakolof Bay ($n = 2812$) and $7.2 \pm 6.5 \mu\text{atm}$ in



Windy Bay ($n = 2854$). From the beginning of the transitional period to kelp harvest, the absolute difference in seawater $p\text{CO}_2$ at the inside mooring versus the outside mooring ranged between 0.1 to 2500.3 μatm in Jakolof Bay (186.0 ± 312.3 μatm , $n = 522$), 0.001 to 127.2 μatm in Kalsin Bay (35.2 ± 18.4 , $n = 2133$), and 0.01 to 147.1 μatm in Windy Bay (26.3 ± 23.2 μatm , $n = 1145$). $p\text{CO}_2$ was lower at the inside mooring than the outside mooring during this later part of the deployments in Jakolof Bay and Kalsin Bay, whereas values at the inside mooring exceeded those of the outside mooring in Windy Bay (Fig. 4). In short, the differences in $p\text{CO}_2$ between the moorings increased as the kelp growing season progressed.

3.2 Air-sea CO_2 flux timeseries

Air-sea CO_2 flux estimations (FCO_2) for all sites and moorings demonstrated a flux of CO_2 from the ocean to the atmosphere during the net heterotrophic period indicated by AOP (Fig. 3; Fig. 5). The FCO_2 for the outside mooring during this period ranged between -60.3 to 204.0 $\text{mmol m}^2 \text{d}^{-1}$ in Jakolof Bay (6.7 ± 12.3 $\text{mmol m}^2 \text{d}^{-1}$, $n = 2812$) and -6.9 to 125.3 $\text{mmol m}^2 \text{d}^{-1}$ in Windy Bay (5.6 ± 11.1 $\text{mmol m}^2 \text{d}^{-1}$, $n = 2854$). As the period of net heterotrophy ended, Kalsin Bay and Windy Bay became carbon sinks while Jakolof Bay remained as a source of carbon to the atmosphere. The proportional difference in FCO_2 between moorings (i.e., the FCO_2 at the inside mooring divided by the outside mooring) increased at all sites over time (see Fig. A3). FCO_2 at the outside mooring ranged between -61.2 to 2453.5 $\text{mmol m}^2 \text{d}^{-1}$ in Jakolof Bay (43.2 ± 191.3 $\text{mmol m}^2 \text{d}^{-1}$, $n = 652$), -178.5 to 3.2 $\text{mmol m}^2 \text{d}^{-1}$ in Kalsin Bay (-11.5 ± 18.7 $\text{mmol m}^2 \text{d}^{-1}$, $n = 335$), and -101.6 to 45.6 $\text{mmol m}^2 \text{d}^{-1}$ in Windy Bay (-4.7 ± 11.7 $\text{mmol m}^2 \text{d}^{-1}$, $n = 2492$). The astronomical rise in FCO_2 in April at the outside mooring in Jakolof Bay was mirrored at the inside mooring (Fig. 5), though the maximum FCO_2 inside the farm was 222.0 $\text{mmol m}^2 \text{d}^{-1}$, an order magnitude smaller than the largest flux outside the farm. The similarities in the trend at both moorings in Jakolof Bay lend confidence that the ambient water at this site continued to be a source of carbon to the atmosphere in early spring.



260 **Figure 5: The partial Variation in air-sea CO₂ fluxes (FCO₂) across the kelp growing season at three different sites and the net FCO₂ representing the inside versus the outside fluxes.**

The influence of the kelp farms created a carbon sink at Jakolof Bay and Kalsin Bay, but a carbon source at Windy Bay (Fig. 5). Net FCO₂, the difference in FCO₂ at the inside versus outside moorings representing the farm signal, integrated over the entire kelp growing season was $-84,397 \pm 41,374 \text{ mol m}^2$ in Jakolof Bay, $-11,115 \pm 1,331 \text{ mol m}^2$ in Kalsin Bay, and $543 \pm 21 \text{ mol m}^2$ in Windy Bay. The small net positive integrated FCO₂ in Windy Bay was due to equal variation in FCO₂ above and below zero throughout the sensor deployment (Fig. 5). The net FCO₂ across the timeseries was within the same magnitude as those of the outside mooring, indicating that large differences were experienced at the inside and outside moorings of each site.

The inside mooring value corresponded with the spatial samples collected at Kalsin Bay at the time of kelp harvest, while the mooring underestimated the FCO₂ of the farm spatial sampling at Jakolof Bay and Windy Bay (Fig. 6). The spatial surveys at each farm indicated a FCO₂ of $4.1 \pm 0.9 \text{ mmol m}^2 \text{ d}^{-1}$ at Jakolof Bay ($n = 9$), $-15.0 \pm 18.3 \text{ mmol m}^2 \text{ d}^{-1}$ at Kalsin Bay ($n = 8$), and $4.9 \pm 0.7 \text{ mmol m}^2 \text{ d}^{-1}$ at Windy Bay ($n = 9$). The FCO₂ of the sample collected at the outside mooring exceeded the farm samples in Jakolof Bay and Windy Bay, but was lower at Kalsin Bay (Fig. 6). The FCO₂ estimate from the timeseries mooring in Kalsin Bay was within the spread of samples measured discretely at the farm, though one of the discrete bottle samples in the farm was comparable to the outside farm sample (Fig. 6). At Jakolof Bay and Windy Bay, mooring values fell below the range measured discretely at the farm (Fig. 6). This spatial survey demonstrated the homogeneity of FCO₂ at the farm and discrepancy between the mooring timeseries and discrete bottle sample FCO₂.

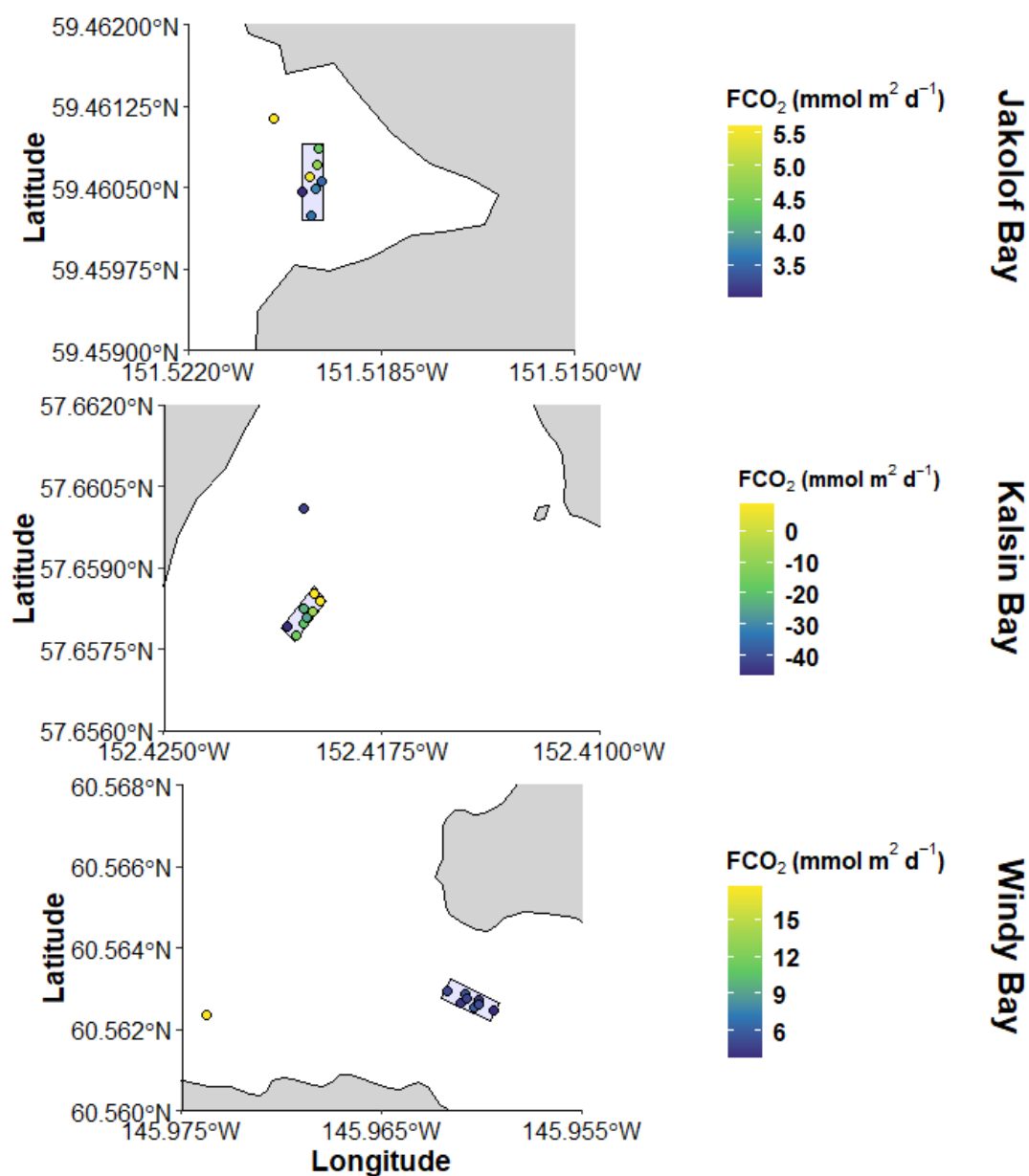


Figure 6: Scatterplot denoting the variation in air-sea CO₂ fluxes (FCO₂) across the kelp farm at three different sites directly right before harvest: April 23 in Jakolof Bay, May 22 in Kalsin Bay, and May 6 in Windy Bay. The light blue rectangle indicates the farm site and the samples taken within this location and the “outside” sample represents the ambient seawater of each bay at a mooring located upstream of the farm.

3.3 Drivers of seawater *p*CO₂

The seawater *p*CO₂ decomposition demonstrated that monthly changes to *p*CO₂ were influenced primarily by biological processes, as both Δ*p*CO₂(DIC) and Δ*p*CO₂(TA) exerted the most considerable change in *p*CO₂ (Fig. 7). DIC and TA applied



both positive and negative changes to $p\text{CO}_2$ depending on site and time during the kelp growing season, but always as opposing forces. As temperature warmed throughout the spring, it decreased the capacity of $p\text{CO}_2$ to remain dissolved in seawater (Fig. 2; Fig. 7). Salinity played a negligible role in $\Delta p\text{CO}_2$ at all sites during all months (Fig. 7). Therefore, the concentration of DIC and TA in seawater, controlled primarily by biological processes, had the greatest influence on $\Delta p\text{CO}_2$, though the $\Delta p\text{CO}_2$ (DIC) term encompasses both water column and benthic processes. Therefore, it is not solely determined by the photosynthesis and respiration occurring in seawater but may also be influenced by benthic biogeochemical fluxes.

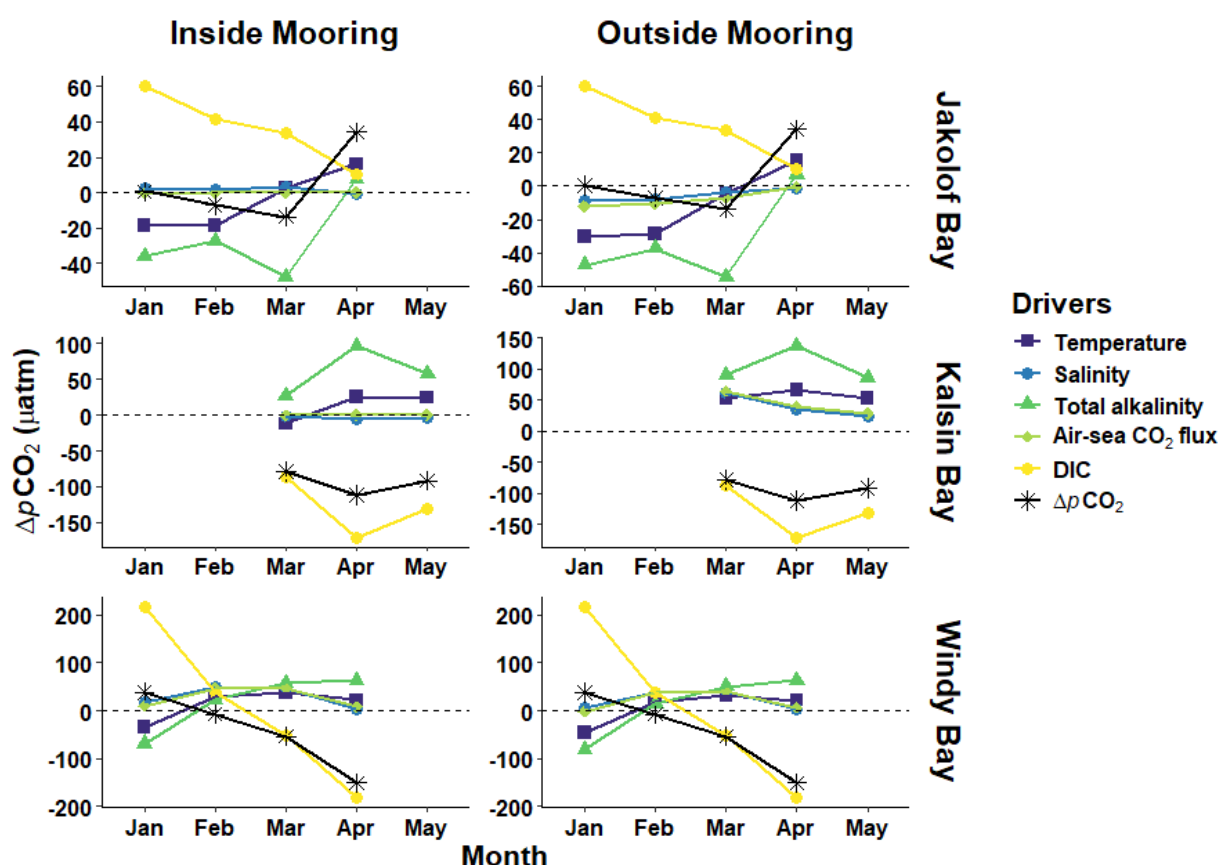


Figure 7: Cumulative monthly changes in $p\text{CO}_2$ due to temperature, salinity, air-sea CO_2 flux, total alkalinity, and dissolved inorganic carbon. The analysis considered December as the starting point for Jakolof Bay and February as the starting point for Kalsin Bay and the prior month was used from thereon to calculate the change in $p\text{CO}_2$ in a given month.

The five drivers used to decompose the monthly changes in seawater $p\text{CO}_2$ did not include all sources of variability. There remained residuals of $-7.6 \mu\text{atm}$, $-4.4 \mu\text{atm}$, $-5.6 \mu\text{atm}$, and $0.4 \mu\text{atm}$ in Jakolof Bay (for January, February, March, and April, respectively), $-4.5 \mu\text{atm}$, $-57.3 \mu\text{atm}$, and $-38.8 \mu\text{atm}$ in Kalsin Bay (for March, April, and May, respectively), and $-104.2 \mu\text{atm}$, $-193.7 \mu\text{atm}$, $-191.0 \mu\text{atm}$, and $-65.9 \mu\text{atm}$ in Windy Bay (for January, February, March, and April,



300 respectively). These residuals suggest that an additional sink of seawater $p\text{CO}_2$ was present but not included as a parameter, and was not captured in decomposition analysis.

The power spectral density (PSD) analysis revealed distinct site-specific and monthly differences in seawater $p\text{CO}_2$ periodicity that suggest diel and tidal cycling to be important drivers particularly as spring progresses (Fig. 8). Frequencies observed at 2 day^{-1} correspond to 12-hour cycles likely driven by tidal forcing. This frequency was strongly apparent in
305 Jakolof Bay, to a lesser degree in Windy Bay, but not at Kalsin Bay (Fig. 8), suggesting that tides play a larger role in $p\text{CO}_2$ variability in Jakolof Bay than either Kalsin Bay or Windy Bay. Frequencies corresponding to 1 day^{-1} , observed at all sites, also indicate a diel periodicity. The most likely driver of a diel cycle would be irradiance, Although temperature and salinity may change as a product of the day/night cycle, the decomposition of $p\text{CO}_2$ indicated that these factors played minimal roles controlling seawater $p\text{CO}_2$ (Fig. 7). The outside mooring in Jakolof Bay demonstrated greater PSD at the tidal periodicity
310 than the diel periodicity, while the opposite was true at the inside mooring, indicating that inside the farm the influence of photosynthesis during the day and respiration at night was stronger than what was observed for ambient seawater. There were multiple peaks $< 1 \text{ day}^{-1}$: 0.3 and 0.7 in Jakolof Bay, 0.3 in Kalsin Bay, and 0.3 and 0.6 in Windy Bay. Frequencies at 0.3, 0.6, and 0.7 day^{-1} correspond to periodicity in seawater $p\text{CO}_2$ every 3.3, 1.6, and 1.4 days. Further, the peaks of PSD grew stronger as the spring progressed with observable peaks beginning in April for Jakolof Bay and Kalsin Bay, and in
315 March for Windy Bay (Fig. 8).

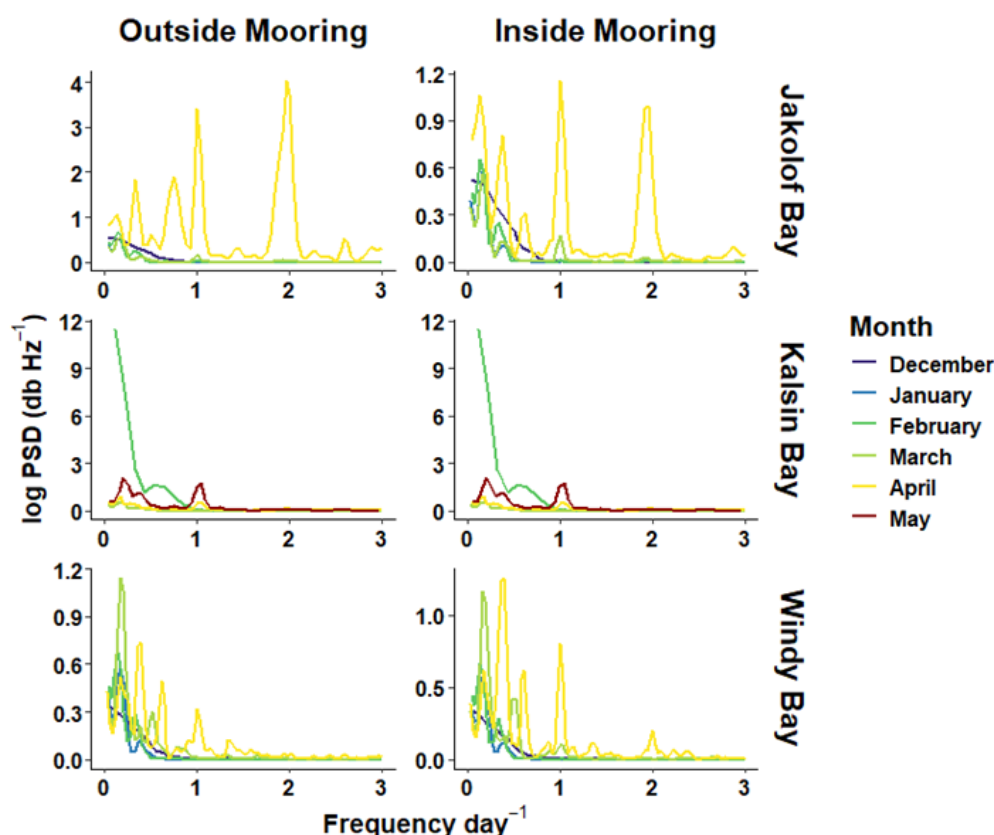


Figure 8: Monthly power spectral density analysis for Jakolof Bay, Kalsin Bay, and Windy Bay, inside and outside of the kelp farm at 3 m depth.

4 Discussion

320 Three kelp farms across the Northern Gulf of Alaska (NGA) varied in the magnitude and direction of their influence on nearshore biogeochemistry. This study directly measured the effect of farmed kelp on the seawater carbonate system using four-to-six-month long sensor deployments recording hourly. Across the kelp growing season, which extends from winter to spring, two of the three farms demonstrated a net negative integrated air-sea CO_2 flux (i.e., carbon moved from the atmosphere to the ocean) (Fig. 5). Biological processes drove the changes in seawater $p\text{CO}_2$, largely on a diel cycle (Fig. 7; 325 Fig. 8). This suggests that carbon sequestration potential of kelp farms in the NGA is site-specific. Results from one site cannot be generalized across the region, highlighting the need for studies that compare CO_2 air-sea flux measurements from multiple sites across a heterogenous coastal landscape.



4.1 Influence of site-specific differences in air-sea CO₂ fluxes (FCO₂)

Each site differed in its response to apparent oxygen production, $p\text{CO}_2$ concentration, air-sea CO₂ flux (FCO₂), and
330 periodicity, demonstrating the need to determine site-specific influences on kelp farm carbon uptake (Fig. 3; Fig. 4; Fig. 5;
Fig. 6; Fig. 7; Fig. 8). All sites in the NGA experienced a shift from net heterotrophy to net autotrophy in spring, with a
transitional period of a few weeks where the system remained near the O₂ solubility compensation point (Fig. 3). The shift
from heterotrophy to autotrophy in Jakolof Bay occurred a month earlier than a previous study from 2017 analyzing the
same bay, though Miller and Kelley (2021) measured seawater 1 m above the seafloor while this study deployed sensors 3 m
335 below the sea surface, suggesting that there may be a delay in shifting from heterotrophy to autotrophy with depth. At two of
the three sites (i.e. Kalsin Bay and Windy Bay), the timing of this shift coincided with the ocean changing from a carbon
source to a carbon sink (Fig. 4). In contrast, Jakolof Bay became a greater source of carbon to the atmosphere in spring,
reaching magnitude fluxes of FCO₂ rarely observed in coastal environments: 2450 mmol m² d⁻¹ in Jakolof Bay versus ~100
mmol m² d⁻¹ in an Arctic lagoon and -131 mmol m² d⁻¹ in the Southern California Bight coastal region (Ikawa and Oechel
340 2015; Miller et al. 2021).

The elevated biofouling of kelp on the mooring structures in Jakolof Bay may have caused the observed elevated FCO₂ by
creating a closed system where the kelp's respiration exceeded its O₂ production. However, synchronous trends in seawater
 $p\text{CO}_2$ values at the inside and outside moorings in Jakolof Bay suggested that the extreme values measured reflect real
conditions (Fig. 4). The exclusion of regular seawater advection near the boundary layer of the sensor electrodes due to the
345 biofouling could drive a wide range of $p\text{CO}_2$ values (Krause-Jensen et al. 2015). The sensors at the other two sites measured
a well-mixed water column. However, the O₂ data measured in Jakolof Bay was similar to Kalsin Bay and Windy Bay (Fig.
3), suggesting that the production of O₂ is similar across sites but that the kelp respiration at Jakolof Bay may have been
heightened. The respiration rate of kelp will often increase relative to its photosynthetic rate in warmer conditions or with
macroalgae-associated microorganisms (Aamot 2011; Kim et al. 2024; Xiong et al. 2024), potentially explaining why
350 seawater $p\text{CO}_2$ in Jakolof Bay became so much higher than the other sites while O₂ remained similar (Fig. 3; Fig. 4). On
average, though, the FCO₂ flux in the NGA proved similar in magnitude to other coastal locations (Jiang et al. 2013; Ikawa
and Oechel 2014; Miller et al. 2021).

This study provided the first estimates of air-sea CO₂ fluxes within an Alaskan kelp farm but cannot differentiate between
species or population level differences. In Jakolof Bay and Windy Bay, both *S. latissima* and *A. marginata* were grown,
355 while only *A. marginata* was grown in Kalsin Bay. Different kelp species exhibit different rates of photosynthesis due to
physiology and diverging adaptations to preferred environment (Van der Loos 2019): *S. latissima* has adapted to low-light
and low-energy environments while *A. marginata* has adapted to the high-energy, wave-exposed intertidal. Additionally,
intraspecific variation in photosynthetic rates between sites may occur, with regional adaptation to local conditions at these
NGA farms that are > 300 km apart (Bruhn et al. 2016).



360 The farming gear and methods implemented at a given site may also have caused observable differences in the effect of
cultured kelp on seawater carbonate chemistry. This study benefitted from studying three established commercial kelp farms,
but the locations differed in farm size, line spacing, and seeded line source, all of which can influence kelp growth
(Boderskov et al. 2021; Lexa Meyer, unpublished). In Kodiak, AK, decreasing the line spacing limited the growth of kelp
blades but resulted in higher total yield (Lexa Meyer, unpublished). Notably, the quality of seeded line produced in
365 hatcheries within the NGA varies significantly as these hatcheries continue to improve production for this nascent industry,
and seeding method directly correlates with final yields (Boderskov et al. 2021). The variability of farming techniques across
locations, paired with site- and species-specific physiology, makes deconvolving the primary drivers of kelp production and
subsequent FCO₂ difficult to achieve.

4.2 Drivers of nearshore carbonate chemistry in kelp farms

370 The short-term periodicity observed in seawater $p\text{CO}_2$ was accounted for by diel and tidal cycling, but the longer “event-
scale” variability visible in almost all of the timeseries have not yet been explained (Fig. 4; Fig. 8; Fig. 9). Across the sites,
this variability spanned 1.4-to-3.3-day intervals with periodicities strengthening in April and May (Fig. 7). Event-scale
variability has previously been attributed to phytoplankton blooms, advection of upwelled water, and wind relaxation
(Kapsenberg and Hofmann 2016). Phytoplankton blooms persist on scales of two to three weeks (Eslinger et al. 2001) and
375 wind/air-sea exchange played a minimal role in driving changes in $p\text{CO}_2$ (Fig. 8), so these variables are likely not driving
observed periodicity (Fig. 9). Short water residence times in recessed bays in the NGA can cause elevated mixing with
offshore water (Haag et al. 2023), and the undersaturated seawater on the continental shelf could act to dilute the inshore
 $p\text{CO}_2$ with mixing (Evans and Mathis 2013). This mixing with offshore water might explain the event-scale periodicity and
remaining residuals from the decomposition of the monthly changes in seawater $p\text{CO}_2$. Windy Bay, in particular,
380 demonstrated elevated residuals from the $p\text{CO}_2$ decomposition, suggesting that our analysis lacked a critical carbon sink at
this site. The greatest difference between Windy Bay and the other two sites is its proximity to the Copper River, the single
largest point source of freshwater in the NGA (Reister et al. 2024). While this study is speculative, further research should
quantify the relative carbon fluxes in these bays and determine how long the effect of the carbon uptake by kelp persists in
these nearshore sites after harvest.

385 While two of the three kelp farms provided a net drawdown of atmospheric CO₂ across the growing season, the hourly FCO₂
varied from being a source to a sink of carbon, sometimes within the same twenty-four-hour period (Fig. 5). Coastal oceans
exhibit strong diel cycles in $p\text{CO}_2$, and the NGA was not an exception (Fig. 8; Torres et al. 2021). The diel
photosynthesis/respiration cycle of primary producers can alter the availability of TA and DIC in seawater, and was the
dominant driver of $p\text{CO}_2$ in the region such that it could drive both positive and negative FCO₂ should seawater $p\text{CO}_2$ rise
390 above and fall below atmospheric CO₂ (Fig. 7; Torres et al. 2021). Wind speed dominates the magnitude of these fluxes,
therefore an increasing differential between seawater and atmospheric CO₂ would still require strong winds to drive FCO₂
(Eq. 1 and 2). However, wind forcing weakens through spring, which can slow air-sea CO₂ equilibration (Stabeno et al.



2004). Therefore, the timing of wind and air-sea CO₂ differentials are important when considering the ability of kelp farms to draw down atmospheric CO₂, as a mismatch between seasonal winds and the farmed kelp growing season would result in a reduction of CO₂ uptake.

4.3 Carbon credit and ocean acidification mitigation

If one were to consider the uptake of carbon from seawater by a kelp farm, with the assumption that the kelp will be removed from the system through harvest, an estimate of carbon credit capacity can be made using the farm dimensions. The FCO₂ within each farm was fairly homogenous at the timepoint sampled (Fig. 6), further bolstering the notion that the timeseries measured at the mooring was representative of the entire farm. To account for the ability of Alaskan farmed kelps to use CO₂ or bicarbonate as a source of carbon, we calculated the carbon credits two ways: we multiplied both the (1) net integrated dissolved inorganic carbon (DIC) and (2) the net integrated FCO₂ between the inside and outside moorings by the area of the farm assuming the kelp occupied a conservative 1 m depth in the water column. Over the growing season this produced an uptake of DIC into kelp tissue of 51,469 tCO₂ eq in Jakolof Bay, 41,151 tCO₂ eq in Kalsin Bay, and 1450 tCO₂ eq in Windy Bay, an atmospheric CO₂ drawdown of 27,851 tCO₂ eq in Jakolof Bay and 1564 tCO₂ eq in Kalsin Bay, and an atmospheric CO₂ release of 286 tCO₂ eq in Windy Bay. To sell farmed kelp as a carbon credit, farmers would be required to prevent the harvested biomass from being remineralized by sinking their product off the continental shelf in locations of periodic or permanent anoxia (Pederson et al. 2021; Duarte et al. 2025), or by other means, which would leave the carbon credits as the sole source of income for farmers choosing this route.

Kelp farms may also act as local refugia against ocean acidification by creating a halo effect of lower pH water in their vicinity, altering the seawater chemistry so that biocalcification is more favorable (Krause-Jensen et al. 2015; Ries et al. 2016). When aragonite is in equilibrium with respect to seawater, the aragonite saturation state (Ω_{arag}) is 1, and seawater Ω_{arag} remained above that value across most of the NGA with the exception of late spring in Jakolof Bay (Fig. 9). The presence of kelp farms increased the aragonite saturation of seawater in Jakolof Bay and Kalsin Bay which may decrease the susceptibility of organisms with calcium carbonate to dissolve, especially during brief windows of opportunity when organisms experience sensitive life stages (Ross et al. 2011). However, in contrast, the Windy Bay kelp farm decreased aragonite saturation (Fig. 9), indicating that this may not be a universal benefit of kelp farms in this region. Another associated benefit could be co-culturing kelp, which increases seawater Ω_{arag} , with shellfish. The halo of buffered seawater around a kelp farm would decrease the dissolution of calcifying shellfish and provide a food source to those bivalves as suspended kelp detritus (Haag et al. 2025). Studies have demonstrated that high food availability may alleviate pressures of ocean acidification (Hettinger et al. 2013; Thomsen et al. 2013).

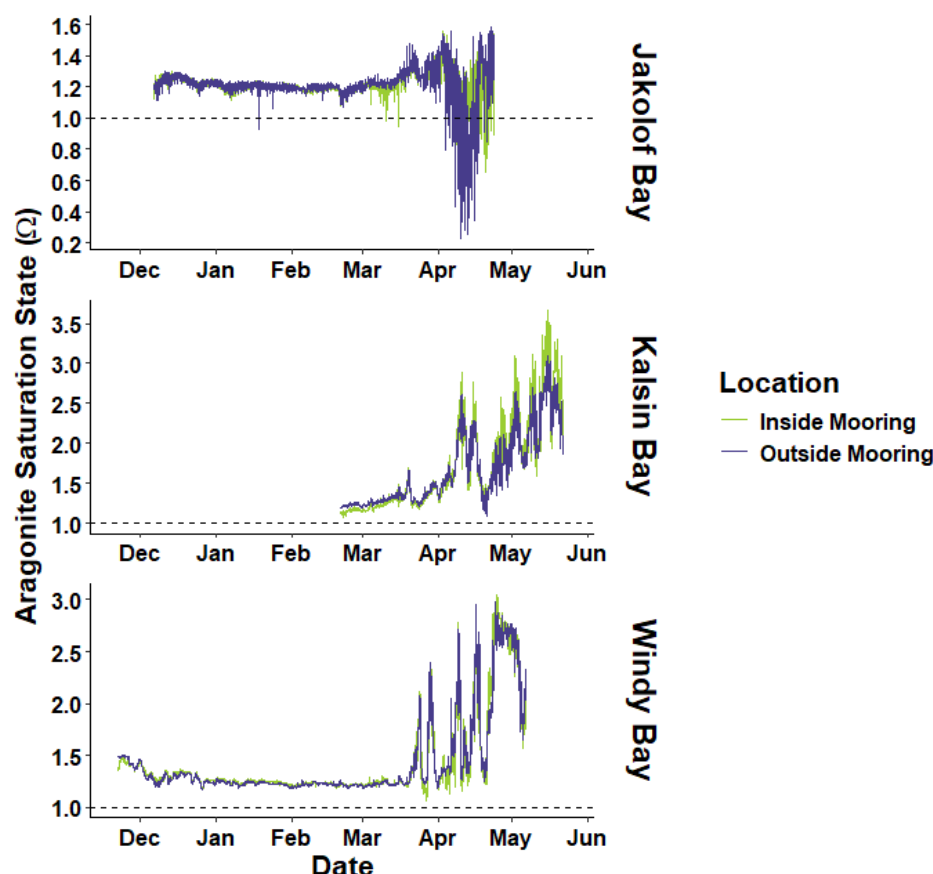


Figure 9: The aragonite saturation in seawater (Ω_{arag}) inside and outside of kelp farms across the kelp growing season in Jakolof Bay, Kalsin Bay, and Windy Bay. The dashed line indicates when seawater is in equilibrium with respect to aragonite ($\Omega_{\text{arag}} = 1$).

425 Estimates of other sources and sinks of kelp-derived carbon in the marine environment are needed to contextualize the effect of farmed kelp. There are extended periods of time during summer where farmed kelp is not present, as it is harvested in early spring and not reseeded until the following winter (Stekoll et al. 2021); however, there are no current estimates in the NGA to the residence time of kelp detritus in the water column. To ascertain the role of kelp farms in carbon cycling, further research should seek to quantify the longevity of kelp influence after harvest and natural drivers of carbon in the nearshore.

430 For example, submarine groundwater discharge plays a dominant role in nutrient cycling in Jakolof Bay due to the high tidal forcing in the area (Haag et al. 2023)—and tides were also demonstrated to be an important driver of seawater $p\text{CO}_2$ (Fig. 8)—but there are no current estimates for advective carbon fluxes at the sediment-water interface.

5 Conclusions

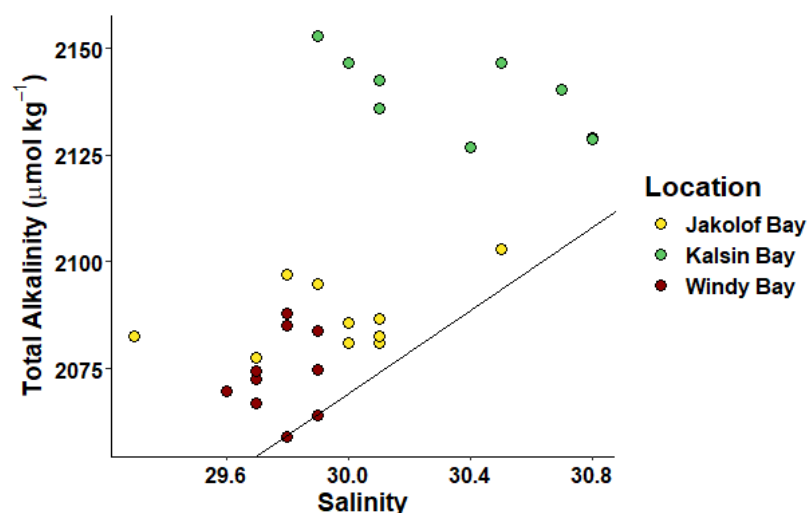
Kelp farms influenced the seawater carbonate chemistry and air-sea CO_2 flux in three bays across the NGA. During the growing season, which extends from winter into late spring, the farmed kelp at two of the three farms increased the capacity

435



for the nearshore to act as a CO_2 sink, while the third farm had the opposite effect. A higher capacity of atmospheric carbon drawdown may be attainable at targeted farm sites where kelp farms increase the carbon sink capacity of the ocean if mariculture activities were to scale, though further studies into intraspecific- and interannual variability would be required to actualize a carbon credit market from Alaska's kelp farming industry.

440 6 Appendix



445 **Figure A1.** The spread of discrete samples taken at the farm sites at the end of the sensor deployments (April 23 in Jakolof Bay, May 22 in Kalsin Bay, and May 6 in Windy Bay) according to their total alkalinity and salinity. The line represents the assumed relationship between total alkalinity and salinity devised by Evans et al. (2015) that was used to convert the salinity timeseries to total alkalinity.



Figure A2. The biofouled moorings retrieved from Jakolof Bay in spring 2024. Wild-set *Alaria marginata* completely encompassed the mooring frames and sensors.

450

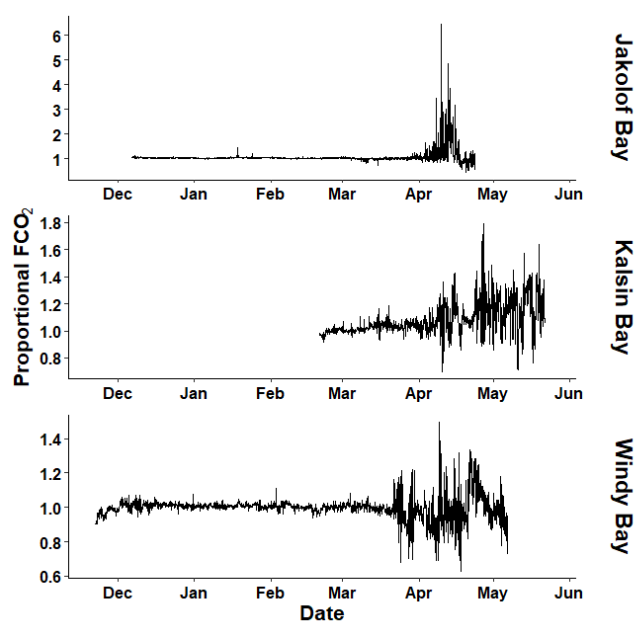


Figure A3. The proportional difference in air-sea CO_2 fluxes (FCO_2) between the inside of a kelp farm relative to ambient conditions at three different sites calculated by dividing the inside mooring by the outside mooring.

455



7 Code availability

The code utilized in this project was minorly modified from pre-existing packages or code already publicly available, so it has not been published anywhere.

8 Data availability

460 Data can be accessed from the DataONE repository (<https://doi.org/10.24431/rw1k9hb>).

9 Author contribution

AK acquired the funding and designed the project with JH. The investigation and data processing was conducted by JH, AK, and JJ. Formal analysis and writing of the original draft was conducted by JH with aid from AK and CM. All authors contributed to the reviewing and editing of the manuscript.

465 10 Competing interests

The authors declare that they have no conflict of interest.

11 Acknowledgments

Samples were collected on the unceded traditional homelands of the Dena'ina, Alutiiq, Eyak, and Sugpiaq and samples were processed on the unceded traditional homelands of the Lower Tanana Dené. Thank you to the kelp farmers who worked with us: Lindsay Olsen and Larry Lansdowne of Spinnaker Sea Farms, Alf Pryor and Lexa Meyer of Alaska Ocean Farms, and
470 Thea Thomas and Cale Herschleb of Royal Ocean Kelp Co. Thank you to Dr. Sarah Mincks, Marina Alcantar, Jonah Jossart, Alorah Bliese, and Emily Ortega for aid in sample collection/processing, data analysis, and manuscript edits. This research was financially supported by the Rasmuson Fisheries Research Center, the Exxon Valdez Oil Spill Mariculture Research and Restoration Consortium, and the Northern Gulf of Alaska Applied Research Award.

475 12 References

Aamot, I. A.: *How photosynthesis in Laminaria digitata and Saccharina latissima is affected by water temperature* MSc thesis, Institutt for biologi, Norwegian University of Science and Technology. <http://hdl.handle.net/11250/244793>, 2011.

Alcantar, M. W., Hetrick, J., Ramsay, J., and Kelley, A. L.: Examining the impacts of elevated, variable $p\text{CO}_2$ on larval Pacific razor clams (*Siliqua patula*) in Alaska, F. in Mar. Sci., 11, 1253702, doi:[10.3389/fmars.2024.1253702](https://doi.org/10.3389/fmars.2024.1253702), 2024.

480 Arzeno-Soltero, I. B., Saenz, B. T., Frieder, C. A., Long, M. C., DeAngelo, J., Davis, S. J., and Davis, K. A.: Large global variations in the carbon dioxide removal potential of seaweed farming due to biophysical constraints, Com. Ear. Env., 4, 185, doi:[10.1038/s43247-023-00833-2](https://doi.org/10.1038/s43247-023-00833-2), 2023.

Bignami, S., Sponaugle, S., and Cowen, R. K.: Response to ocean acidification in larvae of a large tropical marine fish, *Rachycentron canadum*. Glob. Cha. Bio., 19(4), 996-1006, doi:[10.1111/gcb.12133](https://doi.org/10.1111/gcb.12133), 2023.



- 485 Boderskov, T., Nielsen, M. M., Rasmussen, M. B., Balsby, T. J. S., Macleod, A., Holdt, S. L., Sloth, J.J., and Bruhn, A.: Effects of seeding method, timing and site selection on the production and quality of sugar kelp, *Saccharina latissima*: A Danish case study, *Alg. Res.*, 53, 102160, doi:[10.1016/j.algal.2020.102160](https://doi.org/10.1016/j.algal.2020.102160), 2021.
- Bresnahan Jr, P. J., Martz, T. R., Takeshita, Y., Johnson, K. S., and LaShomb, M.: Best practices for autonomous measurement of seawater pH with the Honeywell Durafet, *Meth. in Oce.*, 9, 44-60, doi:[10.1016/j.mio.2014.08.003](https://doi.org/10.1016/j.mio.2014.08.003), 2014.
- 490 Bruhn, A., Tørring, D. B., Thomsen, M., Canal-Vergés, P., Nielsen, M. M., Rasmussen, M. B., Eybye K.L., Larsen, M.M., Balsby, T.J.SI, and Petersen, J. K.: Impact of environmental conditions on biomass yield, quality, and bio-mitigation capacity of *Saccharina latissima*, *Aqu. Env. Inter.*, 8, 619-636, doi:[10.3354/aei00200](https://doi.org/10.3354/aei00200), 2016.
- Bullen, C. D., Driscoll, J., Burt, J., Stephens, T., Hessing-Lewis, M., and Gregr, E. J.: The potential climate benefits of seaweed farming in temperate waters, *Sci. Rep.*, 14(1), 15021, doi:[10.1038/s41598-024-65408-3](https://doi.org/10.1038/s41598-024-65408-3), 2024.
- 495 Cai, W. J.: Estuarine and coastal ocean carbon paradox: CO₂ sinks or sites of terrestrial carbon incineration?, *Ann. Rev. of Mar. Sci.*, 3(1), 123-145, doi:[10.1146/annurev-marine-120709-142723](https://doi.org/10.1146/annurev-marine-120709-142723), 2011.
- Casamitjana, X., and Roget, E.: Resuspension of sediment by focused groundwater in Lake Banyoles. *Limn. and Oce.*, 38(3), 643-656, doi:[10.4319/lo.1993.38.3.0643](https://doi.org/10.4319/lo.1993.38.3.0643), 1993.
- Chen, C. T. A., and Borges, A. V.: Reconciling opposing views on carbon cycling in the coastal ocean: Continental shelves
500 as sinks and near-shore ecosystems as sources of atmospheric CO₂, *Deep Sea Res. Part II: Top. Stud. in Oce.*, 56(8-10), 578-590, doi:[10.1016/j.dsr2.2009.01.001](https://doi.org/10.1016/j.dsr2.2009.01.001), 2009.
- Coleman, S., Dewhurst, T., Fredriksson, D. W., St. Gelais, A. T., Cole, K. L., MacNicoll, M., Laufer, E., and Brady, D. C.: Quantifying baseline costs and cataloging potential optimization strategies for kelp aquaculture carbon dioxide removal, *Front. in Mar. Sci.*, 9, 966304, doi:[10.3389/fmars.2022.966304](https://doi.org/10.3389/fmars.2022.966304), 2022.
- 505 DeAngelo, J., Saenz, B. T., Arzeno-Soltero, I. B., Frieder, C. A., Long, M. C., Hamman, J., Davis, K. A., and Davis, S. J.: Economic and biophysical limits to seaweed farming for climate change mitigation, *Nat. Pla.*, 9(1), 45-57, doi:[10.1038/s41477-022-01305-9](https://doi.org/10.1038/s41477-022-01305-9), 2023.
- Douglas, N. K., and Byrne, R. H.: Achieving accurate spectrophotometric pH measurements using unpurified meta-cresol purple, *Mar. Chem.*, 190, 66-72, doi:[10.1016/j.marchem.2017.02.004](https://doi.org/10.1016/j.marchem.2017.02.004), 2017.
- 510 Duarte, C. M., Delgado-Huertas, A., Marti, E., Gasser, B., Martin, I. S., Cousteau, A., Neumeyer, F., Reilly-Cayten, M., Boyce, J., Kuwae, T., Hori, M., Miyajima, T., Price, N. N., Arnold, S., Ricart, A. M., Davis, S., Surugau, N., Abdul, A., Wu, J., Chung, I. K., Choi, C. G., Sondak, C. F. A., Albasri, H., Krause-Jensen, D., Bruhn, A., Boderskov, T., Hancke, K., Funderud, J., Borrero-Santiago, A. R., Pascal, F., Joanne, P., Ranivoarivelo, L., Collins, W. T., Clark, J., Gutierrez, J. F.,



- Riquelme, R., Avila, M., Macreadie, P. I., and Masque, P.: Carbon burial in sediments below seaweed farms matches that of Blue Carbon habitats, *Nat. Cli. Cha.*, 1-8, doi:[10.1038/s41558-025-02278-1](https://doi.org/10.1038/s41558-025-02278-1), 2025.
- Edgar, G. J., Bates, A. E., Krueck, N. C., Baker, S. C., Stuart-Smith, R. D., and Brown, C. J.: Stock assessment models overstate sustainability of the world's fisheries, *Sci.*, 385(6711), 860-865, doi:[10.1126/science.adl6282](https://doi.org/10.1126/science.adl6282), 2024.
- Eslinger, D. L., Cooney, R. T., Mcroy, C. P., Ward, A., Kline Jr, T. C., Simpson, E. P., Wang, J., and Allen, J. R.: Plankton dynamics: observed and modelled responses to physical conditions in Prince William Sound, Alaska, *Fish, Oce.*, 10, 81-96, doi:[10.1046/j.1054-6006.2001.00036.x](https://doi.org/10.1046/j.1054-6006.2001.00036.x), 2001.
- Evans, W., and Mathis, J. T.: The Gulf of Alaska coastal ocean as an atmospheric CO₂ sink, *Con. S. Res.*, 65, 52-63, doi:[10.1016/j.csr.2013.06.013](https://doi.org/10.1016/j.csr.2013.06.013), 2013.
- Evans, W., Mathis, J. T., Ramsay, J., and Hetrick, J. On the frontline: Tracking ocean acidification in an Alaskan shellfish hatchery, *P. One*, 10(7), e0130384, doi:[10.1371/journal.pone.0130384](https://doi.org/10.1371/journal.pone.0130384), 2015.
- Feely, R. A., Sabine, C. L., Lee, K., Berelson, W., Kleypas, J., Fabry, V. J., and Millero, F. J.: Impact of anthropogenic CO₂ on the CaCO₃ system in the oceans, *Sci.*, 305(5682), 362-366, doi:[10.1126/science.1097329](https://doi.org/10.1126/science.1097329), 2004.
- Gattuso, J.P., Epitalon, J.M., Lavigne, H., Orr, J., Gentili, B., Hagens, M., Hofmann, A., Mueller, J.D., Proye, A., Rae, J. and Soetaert, K.: Package 'seacarb'. doi:10.32614/CRAN.package.seacarb, 2015.
- Gattuso, J.P., Epitalon, J.M., Lavigne, H., Orr, J., Gentili, B., Hagens, M., Hofmann, A., Mueller, J.D., Proye, A., Rae, J. and Soetaert, K., 2015. Package 'seacarb'. *Preprint at [http://cran.r-project.org/package= seacarb](http://cran.r-project.org/package=seacarb)*.
- Garcia, H. E., and Gordon, L. I.: Oxygen solubility in seawater: Better fitting equations, *Lim. and Oce.*, 37(6), 1307-1312, doi:[10.4319/lo.1992.37.6.1307](https://doi.org/10.4319/lo.1992.37.6.1307), 1992.
- García-Troche, E. M., Morell, J. M., Meléndez, M., and Salisbury, J. E.: Carbonate chemistry seasonality in a tropical mangrove lagoon in La Parguera, Puerto Rico, *P. One*, 16(5), e0250069, doi:[10.1371/journal.pone.0250069](https://doi.org/10.1371/journal.pone.0250069), 2021.
- Haag, J., Dulai, H., and Burt, W.: The role of submarine groundwater discharge to the input of macronutrients within a macrotidal subpolar estuary, *Est. and Coa.*, 46(7), 1740-1755, doi:10.1007/s12237-023-01231-9, 2023.
- Haag, J., Mincks, S. L., Jossart, J., and Kelley, A. L.: Seasonal trophic resource partitioning by Pacific oyster *Crassostrea gigas* and Pacific blue mussel *Mytilus trossulus* in an Alaskan estuary, *Mar. Eco. Prog. Ser.*, 754, 65-76, doi:[10.3354/meps14779](https://doi.org/10.3354/meps14779), 2025.
- Hettinger, A., Sanford, E., Hill, T. M., Hosfelt, J. D., Russell, A. D., and Gaylord, B.: The influence of food supply on the response of Olympia oyster larvae to ocean acidification, *Biogeosci.*, 10(10), 6629-6638, doi:10.5194/bg-10-6629-2013, 2013.



- Ikawa, H., and Oechel, W. C. Temporal variations in air-sea CO₂ exchange near large kelp beds near San Diego, California, *Jou. of Geophys. Res.: Oce.*, 120(1), 50-63, doi:[10.1002/2014JC010229](https://doi.org/10.1002/2014JC010229), 2015.
- 545 IPCC.: *Climate Change 2022: Impacts, Adaptation, and Vulnerability*. Contribution of Working Group II to the Sixth Assessment Report of the Intergovernmental Panel on Climate Change, Cambridge University Press, Cambridge, UK and New York, NY, USA, doi:[10.1017/9781009325844](https://doi.org/10.1017/9781009325844), 2022.
- Jiang, Z., Fang, J., Mao, Y., Han, T., and Wang, G.: Influence of seaweed aquaculture on marine inorganic carbon dynamics and sea-air CO₂ flux, *Jou. of the Wor. Aqu. Soc.*, 44(1), 133-140, doi:[10.1111/jwas.12000](https://doi.org/10.1111/jwas.12000), 2013.
- 550 Jiang, Z., Li, J., Qiao, X., Wang, G., Bian, D., Jiang, X., Liu, Y., Huang, D., Wang, W., and Fang, J.: The budget of dissolved inorganic carbon in the shellfish and seaweed integrated mariculture area of Sanggou Bay, Shandong, China, *Aqua.*, 446, 167-174, doi:[10.1016/j.aquaculture.2014.12.043](https://doi.org/10.1016/j.aquaculture.2014.12.043), 2015.
- Kaiser, D. Davidatlarge/ggTS: ggTS first release (v1.0.0). Zenodo, doi:[10.5281/zenodo.3901308](https://doi.org/10.5281/zenodo.3901308), 2020.
- Kapsenberg, L., and Hofmann, G. E.: Ocean pH time-series and drivers of variability along the northern Channel Islands, 555 California, USA. *Limn. and Oce.*, 61(3), 953-968, doi:[10.1002/lno.10264](https://doi.org/10.1002/lno.10264), 2016.
- Kelley D., Richards C., and SCOR/IAPSO W.: `_gsw: Gibbs Sea Water Functions_`. R package version 1.2-0, <https://CRAN.R-project.org/package=gsw>, 2024.
- Kim, J. H., Moon, H., Han, M. J., Jung, J. E., Lee, N. Y., Kang, J. W., Oh, J. C., Park, G., Lee, S., Lee, M., Park, C., Yoon, H., and Kim, H. The photosynthetic uptake of inorganic carbon from *Pyropia seaweed* aquaculture beds: Scaling up 560 population-level estimations, *Aqua.*, 593, 741293, doi: [10.1016/j.aquaculture.2024.741293](https://doi.org/10.1016/j.aquaculture.2024.741293), 2024.
- Krause-Jensen, D., Duarte, C. M., Hendriks, I. E., Meire, L., Blicher, M. E., Marbà, N., and Sejr, M. K.: Macroalgae contribute to nested mosaics of pH variability in a subarctic fjord. *Biogeosci.*, 12(16), 4895-4911, doi:10.5194/bg-12-4895-2015, 2015.
- Kurihara, H., Yin, R., Nishihara, G. N., Soyano, K., and Ishimatsu, A.: Effect of ocean acidification on growth, gonad 565 development and physiology of the sea urchin *Hemicentrotus pulcherrimus*. *Aqu. Bio.*, 18(3), 281-292, doi:[10.3354/ab.2013](https://doi.org/10.3354/ab.2013), 2013.
- Lewis, E. R., and Wallace, D. W. R.: Program developed for CO₂ system calculations. Environmental System Science Data Infrastructure for a Virtual Ecosystem (ESS-DIVE)(United States), doi: [10.15485/1464255](https://doi.org/10.15485/1464255), 1998.
- Ligges, U., Short, T., Kienzle, P., Schnackenberg, S., Billingham, D., Borchers, H.W., Carezia, A., Dupuis, P., Eaton, J.W., 570 Farhi, E., Habel, K., Hornik, K., Krey, S., Lash, B., Leisch, F., Mersmann, O., Neis, P., Ruohio, J., Smith III, J. O., Stewart, D., Weingessel, A.: Package ‘signal’. R Found. for Stat. Comp., doi:10.32614/CRAN.package.signal, 2015.



- Long, W. C., Swiney, K. M., and Foy, R. J.: Effects of ocean acidification on the embryos and larvae of red king crab, *Paralithodes camtschaticus*. Mar. Poll. Bull., 69(1-2), 38-47, doi:[10.1016/j.marpolbul.2013.01.011](https://doi.org/10.1016/j.marpolbul.2013.01.011), 2013.
- MacIntyre, S.: Trace gas exchange across the air-sea interface in fresh water and coastal marine environments. Biogen. Tr. Gases: Meas. Emi. From S. And W., 52-97, <https://cir.nii.ac.jp/crid/1571698600697327104>, 1995.
- McKain, K., Sweeney, C., Baier, B., Crotwell, A., Crotwell, M., Handley, P., Higgs, J., Legard, T., Madronich, M., Miller, J. B., Moglia, E., Mund, J., Newberger, T., Wolter, S., and NOAA Global Monitoring Laboratory.: NOAA Global Greenhouse Gas Reference Network Flask-Air PFP Sample Measurements of CO₂, CH₄, CO, N₂O, H₂, SF₆ and isotopic ratios collected from aircraft vertical profiles [Data set]. Version: 2024-08-12. doi:[10.15138/39HR-9N34](https://doi.org/10.15138/39HR-9N34), (Accessed 12/6/2024).
- 580 Miller, C. A., Pocock, K., Evans, W., and Kelley, A. L.: An evaluation of the performance of Sea-Bird Scientific's SeaFET™ autonomous pH sensor: considerations for the broader oceanographic community. Oce. Sci., 14(4), 751-768, doi:10.5194/os-14-751-2018, 2018.
- Miller, L.: Legalizing local: Alaska's unique opportunity to create an equitable and sustainable seaweed farming industry. Alaska L. Rev., 38, 313-340, 2021.
- 585 Miller, C. A., Bonsell, C., McTigue, N. D., and Kelley, A. L.: The seasonal phases of an Arctic lagoon reveal the discontinuities of pH variability and CO₂ flux at the air-sea interface. Biogeosci., 18(3), 1203-1221, doi:10.5194/bg-18-1203-2021, 2021.
- Miller, C. A., and Kelley, A. L.: Seasonality and biological forcing modify the diel frequency of nearshore pH extremes in a subarctic Alaskan estuary, Limn. and Oce., 66(4), 1475-1491, doi:[10.1002/lno.11698](https://doi.org/10.1002/lno.11698), 2021.
- 590 NOAA National Wind Buoy. <https://www.ndbc.noaa.gov/>, (Accessed 12/26/2024)
- Mongin, M., Baird, M. E., Hadley, S., and Lenton, A.: Optimising reef-scale CO₂ removal by seaweed to buffer ocean acidification. Env. Res. Let., 11(3), 034023, doi:10.1088/1748-9326/11/3/034023, 2016.
- Oschlies, A., Bach, L. T., Fennel, K., Gattuso, J. P., and Mengis, N.: Perspectives and challenges of marine carbon dioxide removal. Front. in Cli., 6, 1506181, doi:[10.3389/fclim.2024.1506181](https://doi.org/10.3389/fclim.2024.1506181), 2025.
- 595 Pedersen, M. F., Filbee-Dexter, K., Frisk, N. L., Sárossy, Z., and Wernberg, T.: Carbon sequestration potential increased by incomplete anaerobic decomposition of kelp detritus. Mar. Eco. Prog. Ser., 660, 53-67, doi:<https://doi.org/10.3354/meps>, 2021.
- Quéré, C., Andrew, R. M., Friedlingstein, P., Sitch, S., Hauck, J., Pongratz, J., Pickers, P. A., Korsbakken, J. I., Peters, G. P., Canadell, J. G., Arneeth, A., Chevallier, F., Chini, L. P., Ciais, P., Doney, S. C., Gkritzalis, T., Goll, D. S., Harris, I., Haverd, V., Hoffman, F. M., Hoppema, M., Houghton, R. A., Hurtt, G., Ilyina, T., Jain, A. K., Johannessen, T., Jones, C. D., Kato, E., Keeling, R. F., Goldewijk, K. K., Landschützer, P., Lefèvre, N., Lienert, S., Liu, Z., Lombardozi, D., Metzl, N., Munro,
- 600



- D. R., Nabel, J. E. M. S., Nakaoka, S., Neill, C., Olsen, A., Ono, T., Patra, P., Peregon, A., Peters, W., Peylin, P., Pfeil, B., Pierrot, D., Poulter, B., Rehder, G., Resplandy, L., Robertson, E., Rocher, M., Rödenbeck, C., Schuster, U., Schwinger, J., Séférian, R., Skjelvan, I., Steinhoff, T., Sutton, A., Tans, P. P., Tian, H., Tilbrook, B., Tubiello, F. N., van der Laan-Luijkx, I. T., van der Werf, G. R., Viovy, N., Walker, A. P., Wiltshire, A. J., Wright, R., Zaehele, S., and Zheng, B.: Global carbon budget 2018, *Ear. Sys. Sci. Data.*, 10, 2141-2194, doi:10.5194/essd-10-2141-2018, 2018.
- Reister, I., Danielson, S., and Aguilar-Islas, A.: Perspectives on Northern Gulf of Alaska salinity field structure, freshwater pathways, and controlling mechanisms, *Prog. in Oce.*, 103373, doi:10.1016/j.pocan.2024.103373, 2024.
- Ries, J. B., Ghazaleh, M. N., Connolly, B., Westfield, I., and Castillo, K. D.: Impacts of seawater saturation state ($\Omega_A = 0.4$ –4.6) and temperature (10, 25 C) on the dissolution kinetics of whole-shell biogenic carbonates, *Geochi. et Cosmochi. A.*, 192, 318-337, doi:10.1016/j.gca.2016.07.001, 2016.
- Ross, P. M., Parker, L., O'Connor, W. A., and Bailey, E. A.: The impact of ocean acidification on reproduction, early development and settlement of marine organisms, *Wat.*, 15(11), doi:10.3390/w3041005, 2011.
- Stabeno, P. J., Bond, N. A., Hermann, A. J., Kachel, N. B., Mordy, C. W., and Overland, J. E.: Meteorology and oceanography of the Northern Gulf of Alaska, *Cont. Shelf Res.*, 24(7-8), 859-897, doi:10.1016/j.csr.2004.02.007, 2004.
- Stekoll, M. S., Peeples, T. N., and Raymond, A. E.: Mariculture research of *Macrocystis pyrifera* and *Saccharina latissima* in Southeast Alaska, *Jour. of the Wor. Aqua. Soc.*, 52(5), 1031-1046, doi:10.1111/jwas.12765, 2021.
- Thomsen, J., Casties, I., Pansch, C., Körtzinger, A., and Melzner, F.: Food availability outweighs ocean acidification effects in juvenile *Mytilus edulis*: laboratory and field experiments, *Glob. Cha. Bio.*, 19(4), 1017-1027, doi:10.1111/gcb.12109, 2013.
- Torres, O., Kwiatkowski, L., Sutton, A. J., Dorey, N., and Orr, J. C.: Characterizing mean and extreme diurnal variability of ocean CO₂ system variables across marine environments, *Geophys. Res. Lett.* 48(5), e2020GL090228, doi:10.1029/2020GL090228, 2021.
- Trapletti, A., Hornik, K., LeBaron, B., and Hornik, M. K.: Package 'tseries'. R proj. doi: 10.32614/CRAN.package.tseries, 2015.
- John, C. R., and Watson, D.: Spectrum: Fast Adaptive Spectral Clustering for Single and Multi-View Data, doi:10.32614/CRAN.package.Spectrum, 2020.
- van der Loos, L. M., Schmid, M., Leal, P. P., McGraw, C. M., Britton, D., Revill, A. T., Virtue, P., Nichols, P. D., and Hurd, C. L.: Responses of macroalgae to CO₂ enrichment cannot be inferred solely from their inorganic carbon uptake strategy. *Eco. and Evol.*, 9(1), 125-140, doi:10.1002/ece3.4679, 2019.



Wanninkhof, R. Relationship between wind speed and gas exchange over the ocean revisited. *Limn. and Oce.: Met.*, 12(6), 351-362, doi:[10.1029/92JC00188](https://doi.org/10.1029/92JC00188), 2014.

Williams, C. R., Dittman, A. H., McElhany, P., Busch, D. S., Maher, M. T., Bammler, T. K., MacDonald, J. W., and Gallagher, E. P.: Elevated CO₂ impairs olfactory-mediated neural and behavioral responses and gene expression in ocean-phase coho salmon (*Oncorhynchus kisutch*), *Glob. Cha. Bio.*, 25(3), 963-977, doi:[10.1111/gcb.14532](https://doi.org/10.1111/gcb.14532), 2019.

Xiong, T., Li, H., Hu, Y., Zhai, W. D., Zhang, Z., Liu, Y., Zhang, J., Lu, L., Chang, L., Xe, L., Wei, Q., Jiao, N., and Zhang, Y.: Seaweed farming environments do not always function as CO₂ sink under synergistic influence of macroalgae and microorganisms. *Agr., Eco. & Env.*, 361, 108824, doi:[10.1016/j.agee.2023.108824](https://doi.org/10.1016/j.agee.2023.108824), 2024.